Negative-Valence Neurons in the Larval Zebrafish Pallium

Colton D. Smith[1,2], Zhuowei Du[1,3], William P. Dempsey[1], Scott E. Fraser[1,3,4,5], Thai V. Truong[1,3,4] and Don B. Arnold[1,4,5]

1. Department of Biological Sciences, Division of Molecular and Computational Biology, University of Southern California, Los Angeles, CA 90089
2. Neuroscience Graduate Program, University of Southern California, Los Angeles, CA 90089
3. Translational Imaging Center, University of Southern California, Los Angeles, CA 90089
4. Viterbi School of Engineering, University of Southern California, Los Angeles, CA 90089
5. Department of Quantitative and Computational Biology, University of Southern California, Los Angeles, CA 90089

Abstract:

An organism's survival depends on the rapid classification of sensory events as either harmful or beneficial. In mammals, this computation is partially performed by neurons in the amygdala that respond to signals with negative or positive valence. The larval zebrafish pallium is thought to contain homologs of the mammalian amygdala,

isocortex, and hippocampus; however, the signals encoded by pallial neurons remain largely uncharacterized. Using two-photon light-sheet microscopy to image 7–9-day-old zebrafish that express pan-neuronal GCaMP6s, we recorded calcium dynamics throughout the brain while presenting a panel of strongly aversive stimuli including infrared heat, electric shock, and a whole-field looming shadow, together with milder threats including vibration, loud sound, light transitions, and a partial looming stimulus. A compact cluster of neurons in the rostrolateral dorsal pallium (Rl) responded vigorously to strongly noxious and fully looming stimuli, but not to the milder cues. In contrast, neurons in the ventromedial pallium and habenula responded to all stimuli tested. Rl neurons are characterized by high Tiam2a expression, suggesting they can be genetically accessed. Thus, our results identify a locus of negative valence neurons in the teleost pallium.

Introduction

To evaluate potential threats, organisms must predict future events based on sensory cues (Herberholz and Marquart, 2012). For example, when a predator approaches a fish, sudden changes in water pressure activate its lateral line system, which, combined with visual cues, allows it to predict that danger is imminent and swiftly evade the threat (Olszewski et al., 2012). How fish decide to flee, or, conversely, to mate or feed, remains poorly understood. In mammals, several lines of evidence suggest that this process involves the basolateral amygdala, where distinct ensembles encode negative and positive value (Beyeler et al., 2018; Grewe et al., 2017; Namburi et al., 2015; Tye, 2018; Xiu et al., 2014). Lesions or chemogenetic silencing of the amygdala blunt defensive behaviors and block fear conditioning (Bechara et al., 2003; Corder et al.,

46 2019; Downer, 1961; Feinstein et al., 2011; LeDoux et al., 1988; Phillips and LeDoux,
47 1992). The amygdala is also a locus of synaptic change following fear learning (Clem
48 and Huganir, 2010; Goosens and Maren, 2002; Nabavi et al., 2014; Phillips and
49 LeDoux, 1992; Quirk et al., 1995; Rogan et al., 1997). Finally, neurons in the basolateral
50 amygdala project differentially depending on their valence, with negative-valence
51 neurons projecting to the medial central amygdala and neighboring positive-valence
52 neurons projecting to the nucleus accumbens, consistent with activation of the two sets
53 of neurons causing distinct downstream effects (Beyeler et al., 2018; Fadok et al., 2017;
54 Penzo et al., 2014; Tye et al., 2011).
55
56 The larval zebrafish (Danio rerio) is an excellent model system for studying sensory
57 processing because its transparent brain is amenable to whole-brain imaging paradigms
58 that require low scattering, such as selective plane illumination microscopy (SPIM;
59 Ahrens et al., 2013). The high speed of SPIM and its low toxicity enable 4-D imaging
60 across large areas of the larval zebrafish brain (Vladimirov et al., 2018). Furthermore, a
61 modified SPIM that uses two-photon excitation (Truong et al., 2011) significantly
62 reduces toxicity and increases penetration relative to 1-P SPIM. Although its brain is
63 smaller and less complex than those of many other vertebrates, the zebrafish can, even
64 in its larval stage, learn to modify responses to environmental stimuli (Gerlai, 2011). In
65 particular, zebrafish are amenable to classical conditioning, which in some cases
66 depends on distinct regions in the telencephalon (Lal et al., 2018; M Portavella et al.,
67 2004; Portavella et al., 2002; Ruhl et al., 2015). Previously, we showed that a well-
68 defined area in the rostrolateral pallium (Rl) contains neurons that respond to aversive

69 heating (Dempsey et al., 2022), suggesting that RI, like the mammalian amygdala, may
70 contain negative-valence neurons.
71
72 To characterize how neurons in the forebrain of a larval zebrafish respond to sensory
73 stimuli of different valence, we mapped GCaMP (a genetically encoded Ca^{2+} indicator)
74 fluorescence following exposure of the fish to stimuli ranging from highly threatening to
75 mildly aversive. We found a tightly clustered group of neurons in RI that responded
76 vigorously to negative-valence stimuli that are highly predictive of tissue damage, but
77 not to less intense negative-valence stimuli. Two additional areas, the ventromedial
78 pallium (Vm) and the habenula (Hb), contained neurons that responded to both types of
79 stimuli. Negative-valence neurons in RI specifically expressed *tiam2a*, a homolog of a
80 gene expressed in the mouse hippocampus. Thus, we have identified a set of negative-
81 valence neurons within the zebrafish pallium that express a unique molecular marker.

82 **Results**

83 *Noxious stimuli activate pallial neurons*
84 To investigate how neurons in the forebrain respond to negative-valence stimuli, we
85 created a transgenic zebrafish line, Tg[CAG_{NRSE}:GCaMP6s], expressing GCaMP6s
86 (Chen et al., 2013)driven by the chicken β-Actin CAG promoter (Quitschke et al., 1989)
87 with an NRSE repressor element (Bergeron et al., 2012) added to diminish expression
88 in non-neuronal cells. Wholemount immunostaining for GCaMP6s and the neuronal
89 marker HuC (elav3) in the forebrain of a 7 dpf Tg[CAG_{NRSE}:GCaMP6s] zebrafish shows
90 almost complete overlap of the two labels, suggesting that virtually all neurons in the

91 zebrafish pallium express GCaMP6s (**Fig. S1**). Note that some skin cells expressed
92 GCaMP6s and were thus excluded from all analyses.
93
94 To explore the pallial responses to negative-valence stimuli in real time, we imaged the
95 Tg[CAG_{NRSE}:GCaMP6s] zebrafish using a custom-built two-photon (2P) SPIM
96 (Keomanee-Dizon et al., 2020) (**Fig. S2**). The 2P-SPIM microscope generates a 2P-
97 excitation light sheet using ultrafast near-infrared laser pulses. This microscope
98 combines non-linear excitation for high penetration depth with orthogonal light-sheet
99 illumination for high acquisition speed and low photodamage (Truong et al., 2011). We
100 immobilized 7–9 dpf fish by embedding them in agarose and placing them in a holder
101 immediately adjacent to the SPIM's two objectives (**Fig. S2**).
102
103 In our initial studies, we exposed the fish to noxious infrared (IR) heating from a laser
104 positioned over the zebrafish's right eye (**Figs. S2, 1A**), which we previously found
105 elicited a strong escape response consisting of a tail flick (Dempsey et al., 2022). The
106 IR stimulus consisted of a series of five 2-second pulses with 2-minute intervals
107 between. Before, during, and after the stimulus, the SPIM imaged a series of optical
108 sections at 11 depths spanning 60 mm, acquired sequentially every 0.12 seconds,
109 completing a stack every 1.33 seconds. We found that three discrete areas in each
110 hemisphere of the zebrafish forebrain showed an overall increase in fluorescence
111 ($\Delta F/F$, see methods) in response to the IR stimulus (**Fig. 1B**). These areas correspond
112 to the left and right Hb (lHb and rHb), left and right RI (lRI and rRI), and left and right Vm
113 (lVm and rVm) (**Fig. S3**). Time-lapse images of fluorescent signals (with background

114 measured before the stimulus subtracted) show an abrupt increase shortly after the
115 stimulus, with average ΔF/F increasing significantly in each of the six areas (**Fig. 1C-E**,
116 n = 5 fish).
117
118 To characterize the response of pallial and habenular neurons more fully, we exposed
119 the fish to electric shock, another noxious stimulus. We used wires placed
120 approximately 1 mm from the otic vesicles (the ears) to deliver 500 mA of current for
121 400 ms (**Fig. 1F**). All six brain regions that increased activity with IR stimulation also
122 showed a qualitative increase in activity following the electric shock (**Fig. 1G, H**). In
123 addition, the average ΔF/F, measured after electric shock, was significantly higher than
124 measurements before the shock (n = 5 fish**, Fig. 1I, J**). These results show that the Hb,
125 RI, and Vm areas of the pallium bilaterally respond to two different noxious stimuli.
126
127 To better understand activity at the level of individual neurons, we used the Ca^{2+} signal
128 detection program CaImAn (Giovannucci et al., 2019) to extract neuronal responses
129 from the raw fluorescence data (see methods). Because the CaImAn program cannot
130 reliably distinguish signals from axons, dendrites, and somata, the signals may not
131 represent distinct cells; thus, we refer to the traces produced by CaImAn as "neuronal
132 components". We counted the number of neuronal components with averaged ΔF/F
133 responses that increased by 50% or more compared with before the stimulus, which we
134 refer to as "activated", and those that decreased by 50% or more, which we refer to as
135 "inhibited" (**Fig. 2A, B**). In response to IR heating, the ratio of activated to inhibited
136 neuronal components (A/I) was 5.0 for Hb, 2.0 for RI, and 4.8 for Vm (**Fig. 2C**).

137 Similarly, responses to electric shock had A/I ratios of 2.8 for Hb, 1.8 for RI, and 4.0 for
138 Vm (**Fig. 2D**).
139
140 Although it was not possible to expose the fish to multiple stimuli within a single imaging
141 session due to their fragility, we plotted the cumulative distribution of activated vs.
142 inhibited neuronal components onto a canonical fish template for both IR heating and
143 electric shock so that we could compare responses to the two stimuli (**Fig. 2C, D**). In RI,
144 components activated by both IR heating and electric shock were generally located in
145 the same region, caudal and medial to the region containing inhibited components.
146
147 **Distinct responses to full and partial looming stimuli in RI**
148 Given that two different noxious stimuli evoked activity in Hb, RI, and Vm (**Figs. 1, 2**),
149 we asked how the same regions would respond to a non-noxious stimulus that still
150 indicated an imminent threat of bodily harm. For many visual species, including
151 zebrafish, a looming stimulus consisting of a black disc that increases in size, mimicking
152 the shadow of an approaching predator, signals a potential threat and triggers
153 evolutionarily hard-wired defensive behaviors like freezing or fleeing (Neo et al., 2015).
154 To generate a looming stimulus, we projected a black disc onto a small projector screen
155 located to the right of the 7–9 dpf zebrafish, which started as a 1° point and grew over
156 500 ms to cover the fish's entire visual field. After remaining at full size for 5 s, the disc
157 contracted back to 1°. During this sequence, we monitored GCaMP fluorescence.
158 Similar to exposure to IR heating and electric shock, the full looming stimulus
159 immediately elicited increased activation in all six regions activated by noxious stimuli

160 (**Fig. 3A-C**). There was residual activity in several areas, including rVm, rRl, and lRl 8 s
161 after the stimulus ceased. Quantitation of the average ΔF/F before and after
162 presentations showed significant increases in all six areas (n = 5, **Fig. 3D, E**).
163
164 Given the robust response to the full looming stimulus, we asked whether a similar, but
165 less intense stimulus, might elicit a different neuronal response. Thus, we developed a
166 partial looming stimulus, which is similar to the full looming stimulus, except the disc
167 stops growing after 300 ms when it covers approximately 48 degrees of the visual field,
168 and then, after 5 s, reduces in size over 300 ms to a 1° point, which could mimic a
169 predator that comes close to the fish but then stops (**Fig. 3F**). Strikingly, the partial-
170 looming stimulus did not elicit a significant overall ΔF/F increase in Rl, although
171 increases in activity in Hb and Vm were significant (n = 7, **Fig. 3G-J**).
172
173 A/I ratios of individual activated and inhibited neuronal components responding to the
174 full looming stimulus were 7.2 in Hb, 1.4 in Rl, and 5.5 in Vm, indicating that activation
175 predominated overall (**Fig. 4A**, **C**). However, in response to the partial looming stimulus,
176 neuronal components showed an A/I of 1.2 in Hb and 3.0 in Vm, whereas inhibited
177 components predominated in Rl (A/I = 0.41; **Fig. 4B**, **D**). Thus, multiple measures of
178 neuronal activity are consistent with Rl being activated by noxious stimuli and a full
179 looming stimulus, but not by a partial looming stimulus. In contrast, Vm and Hb are
180 activated by all stimuli tested.
181
182 **Mild negative-valence stimuli do not activate Rl neurons.**

183 To further test whether RI neurons respond only to highly threatening stimuli, such as
184 noxious stimuli, or to a full looming stimulus, we exposed larval zebrafish to stimuli that
185 could be perceived as threatening but do not indicate imminent bodily harm and
186 measured the response in Hb, RI, and Vm. Specifically, we exposed the zebrafish to
187 sudden vibration, loud noises, and a transition from light to darkness. Each of these
188 stimuli has been shown to elicit startle responses, including C-bends, in larval zebrafish
189 (Beppi et al., 2021; Neo et al., 2015), consistent with their being inherently threatening
190 (Bartoszek et al., 2021). To expose the fish to vibration while recording GCaMP activity
191 with the SPIM, we tapped the right side of the imaging chamber with a plastic stick for 5
192 s. We also presented an auditory stimulus by sounding an airhorn that produced a 120-
193 130 dB sound lasting 0.5 s. Finally, fish that had been equilibrated to darkness, then
194 exposed to light for 4 s, followed by an abrupt return to darkness, were analyzed for
195 response to the light-to-dark transition. Each stimulus was repeated 5 times with a 2-
196 min interval between trials. During and after each stimulus, increased activity was
197 apparent in Hb and Vm, whereas no overall activity change was observed in RI (**Fig**.
198 **5A-I**).
199
200 Statistical analysis showed that overall ΔF/F increased significantly in the rHb, lVm, and
201 rVm in response to tapping, but activity in RI did not increase significantly (n = 6 fish,
202 **Fig. 6A, B**). Similar results were found for exposure to the air horn blast, where activity
203 significantly increased in Hb and Vm, but not in RI (n = 4, **Fig. 6C, D**). Finally, overall
204 ΔF/F increased significantly in rHb and lVm, but not in RI, following a dark-to-light
205 transition (n = 5, **Fig. 6E, F**). Consistent with these results, A/I ratios for the neuronal

206 components found in Hb and Vm ranged from 1.6-4.3 but were substantially less than 1
207 (0.29-0.66) in RI for tapping, airhorn, and light-to-dark transitions (**Fig. 7A-F**). Thus,
208 overall activity in Hb and Vm increases significantly in response to moderately
209 threatening stimuli, at least unilaterally, and activated neuronal components outnumber
210 those that are inhibited. In contrast, in RI, overall ΔF/F does not increase significantly,
211 and inhibited neuronal components outnumber activated ones.
212
213 In conclusion, our results suggest that RI responds exclusively to the most threatening
214 stimuli, but not to less threatening stimuli both in terms of overall activity and A/I ratio of
215 neuronal components (**Fig. 8**). In contrast, Hb and Vm respond at least unilaterally to all
216 negative-valence stimuli and neuronal components have A/I ratios > 1 (**Fig. 8**),
217 regardless of whether they are strongly or weakly threatening. Thus, in principle, signals
218 present in RI could be used to identify highly threatening stimuli.
219
220 **Tiam2a-positive neurons in the rostrolateral pallium.**
221 To better understand the properties of neurons in the RI area that respond specifically to
222 imminent threats, we used the MapZebrain cellular-resolution atlas of the larval
223 zebrafish brain (Kunst et al., 2019). We found that in 6 dpf transgenic fish (y264Et, see
224 methods), the *tiam2a* promoter drives GFP specifically in a region of the pallium that
225 matches the location of RI neurons. *tiam2a* is the zebrafish homolog of the mammalian
226 gene *Tiam2*, which encodes a Rac1-associated GEF (Chiu et al., 1999)
227 To test whether *tiam2a* expression is a marker for neurons that respond to threatening
228 stimuli, we exposed 7–9 dpf Tg[tiam2a:GFP] larval zebrafish to heating with an IR laser.

229 Then we performed wholemount immunocytochemistry to detect pERK, a marker of
230 neuronal activity. A projection image of GFP and pERK shows striking colocalization
231 between the two markers, with virtually every GFP+ neuron expressing pERK (**Fig. 9A,**
232 **B**)**.** In contrast, under control conditions with no noxious stimuli present, we observed
233 little pERK expression in GFP+ neurons (**Fig. 9C, D**). To quantify the amount of co-
234 expression between the two, we measured the total intensity of pERK labeling in cells
235 that expressed GFP and subtracted the background intensity of pERK labeling
236 measured in cells in a nearby region of the fish brain that did not express *tiam2a*. pERK
237 labeling in GFP+ cells was ~20-fold higher in the IR Laser exposed group (n = 6) than in
238 the control group (n = 8), a statistically significant difference (one-tailed t-test; **Fig 9E**).
239 These data are consistent with *tiam2a* being a marker for pallial neurons that are more
240 active when zebrafish are exposed to noxious stimuli.
241
242 To investigate the morphology of Rl neurons, we examined Tg[tiam2a:GFP] fish (**Fig.**
243 **9F**). From the dorsal view, GFP-labeled neurons are highly clustered in the rostrolateral
244 pallium, and from the coronal view, they appear superficial and dorsal. Furthermore,
245 they have short axons, suggesting they are involved in local connectivity. Thus, *tiam2a*
246 promoter-mediated expression defines a tightly packed group of neurons that respond
247 to a noxious stimulus in the 7–9 dpf larval zebrafish. These neurons are likely negative-
248 valence neurons that respond specifically to a variety of stimuli indicating a high
249 likelihood of bodily injury, but not to less threatening aversive stimuli.
250

Discussion

In this study, we defined responses of neurons in the larval zebrafish forebrain to noxious stimuli (IR heating and electric shock), non-noxious threatening stimuli (full looming), and less threatening stimuli (partial looming, vibration, loud noise, and dark-to-light transitions). Prior research has shown that in the adult zebrafish, neurons in the pallial area DI, which partially overlaps with RI, drive ongoing habenular activity (Bartoszek et al., 2021). However, dynamic responses of forebrain neurons to negative-valence stimuli have not been reported previously. Here, we have found that noxious and non-noxious threatening stimuli activate a distinct population of tightly clustered neurons within the rostrolateral dorsal pallium (RI). However, neurons within this same region do not respond to less threatening stimuli. In contrast, neurons in the ventromedial pallium and the habenula respond to all the stimuli tested, encompassing both highly threatening and mildly aversive stimuli.

In addition to neuronal components activated by negative-valence stimuli, we found components in RI that exhibited reduced activity upon exposure to noxious and threatening stimuli. Previously, it was found that neurons inhibited by negative-valence stimuli may also be activated by positive valence stimuli, suggesting that these neurons may respond to positive valence (Belova et al., 2008; Smith and Torregrossa, 2021). The ratio of activated to inhibited neuronal components was highly correlated with whether the overall signal from a given region increased in response to a specific stimulus. A/I ratio (number of activated vs. inhibited neuronal components) > 1 was correlated with regional activation, whereas A/I < 1 was associated with a lack of

activation. In the future, it will be important to test positive-valence stimuli to determine whether they elicit responses in neurons inhibited by negative-valence stimuli. Attempts in this study to elicit a response from forebrain neurons to the smell of food, a positive-valence stimulus, were unsuccessful (data not shown). Additionally, it will be important to determine whether individual neurons in Vm and Hb are broadly tuned to negative-valence stimuli or respond to stimuli of all valences.

It is important to emphasize that RI neurons respond to both looming and noxious stimuli. For cells to be classified as negative-valence, they must respond not only to inherently painful stimuli but also to stimuli that are potentially threatening (Pignatelli & Beyeler, 2018). We found that a full-coverage looming shadow activated RI neurons, along with ventromedial and habenular regions, in a manner similar to physically noxious stimuli. However, a partial looming shadow failed to elicit a response in RI, although it activated Hb and Vm. Interestingly, it has been shown that when a zebrafish is exposed to a full looming stimulus that covers all of the visual field, it is likely to freeze, whereas a fish exposed to a looming disc that stops growing when the visual field is only partially covered (**Fig. 3F**), is more likely to try to escape (Temizer et al., 2015). Thus, results from this paper suggest that signals from RI, which responds differentially to full and partial looming stimuli, could contribute to the initiation of appropriate defensive behaviors in response to threats.

In this study, we exploited the unique properties of the larval zebrafish to obtain parallel recordings of neurons throughout the forebrain in response to negative-valence stimuli.

297 One drawback of using larval zebrafish is that they are relatively delicate, making it
298 difficult to present multiple stimuli to the same fish. Consequently, although it is possible
299 to conclude that neurons in RI are likely to respond when the fish is exposed to one of
300 several different stimuli, we cannot conclude that individual neurons respond to more
301 than one stimulus. In addition, it was difficult to relate the stimuli to behavioral
302 responses. Although tail flicks and heart rate were monitored with every response (not
303 shown), there were no uniform responses to specific stimuli. However, electric shock
304 (Kenney et al., 2017; Manuel et al., 2014), looming stimulus (Temizer et al., 2015),
305 vibration (Eaton et al., 2001), loud noise (Eaton et al., 2001; Neo et al., 2015), dark-to-
306 light and light-to-dark transitions (Beppi et al., 2021) all provoked escape behavior when
307 zebrafish were exposed to them in other contexts. It is possible that being encased in
308 agarose, a requirement for SPIM, limited the fish's behavioral responses. In our
309 experiments, and perhaps for agarose-encased zebrafish in other contexts, neural
310 signatures of negative-valence stimuli are stronger and more consistent than behavioral
311 ones. These findings suggest that forebrain activity, particularly in RI, might be a better
312 indicator of the internal state of the zebrafish's brain than behavior. Together, our results
313 suggest that a transgenic zebrafish expressing GCaMP under the *tiam2a* promoter
314 could provide real-time insight into the animal's internal state.
315
316 Several studies have suggested that the dorsomedial pallium in teleost fish, including
317 zebrafish, is the homolog of the amygdala and the dorsolateral pallium is homologous to
318 the hippocampus based on developmental, topological, and molecular arguments
319 (Baker and Wong, 2021; Mueller et al., 2011; von Trotha et al., 2014). In addition, the

320 medial pallium in general and a specific type of pallial neuron were found to be
321 necessary for fear conditioning in zebrafish (Broglio et al., 2005; Lal et al., 2018; Manuel
322 Portavella et al., 2004; Portavella et al., 2002). In contrast, the results from this study
323 and our previous study suggest that RI neurons are similar in some respects to neurons
324 in the mammalian amygdala. For instance, both of our studies show that RI neurons
325 respond to negative-valence stimuli, a response also seen in many neurons in the
326 mammalian amygdala (Beyeler et al., 2018). RI neurons also become responsive to
327 neutral stimuli following a novel form of classical conditioning (Dempsey et al, 2022).
328 Similarly, following fear conditioning, neurons in the mammalian amygdala become
329 responsive to conditioned stimuli that were paired with unconditioned stimuli (Grewe et
330 al., 2017; Zhang and Li, 2018). Finally, neurons within RI exhibit an increase in
331 excitatory synapses following classical conditioning, and amygdalar neurons undergo
332 long term potentiation, consistent with synaptic change, following fear
333 conditioning(Rogan et al., 1997). However, unlike the amygdala, where negative- and
334 positive-valence neurons are distributed in a salt and pepper fashion (Beyeler et al.,
335 2018), the negative-valence cells that we found in RI tend to be tightly clustered (**Fig. 9**).
336 Furthermore, *tiam2a* is a homolog of mammalian *Tiam2*, which is highly expressed in
337 the hippocampus, and is less abundant in the amygdala in the mouse (Chiu et al.,
338 1999). Thus, our data suggest that RI shares attributes of both the amygdala and the
339 hippocampus, and that teleost fish may have unique brain structures with no exact
340 homologs in mammals.
341

342 **Author contributions**: C.D.S. and D.B.A. designed the experiments and wrote the
343 paper; C.D.S. performed the live-imaging research, contributed new analytic tools, and
344 analyzed data; Z.D. performed the pERK experiments; T.V.T. And S.E.F. supervised the
345 development and maintenance of the SPIM used for live imaging. W.P.D. performed
346 preliminary experiments that were critical for the development of the experimental
347 protocols used in this paper. D.B.A. secured funding and supervised all aspects of the
348 project.
349

350 **Materials and Methods**

351 **Zebrafish husbandry and embryo/larval care**

352 Many of the methods presented in this paper were developed previously (Dempsey et
353 al., 2022). Larval and adult Casper mutant zebrafish were maintained in an in-house
354 veterinary facility in accordance with protocols approved by the University of Southern
355 California (USC) Institutional Animal Care and Use Committee (IACUC). All experiments
356 described in this work were approved by the USC IACUC. Embryos were kept in egg
357 water (1.19 g NaCl, 0.377 g CaSO4·2H2O, 265 mL methylene blue, filled up to 5 liters
358 with ddH_2O) at 28 °C in an incubator with a 13 hr:11 hr light:dark cycle until 5-6 dpf,
359 when they were transferred to tanks within the husbandry facility. On the husbandry
360 system, zebrafish were also maintained on a 13 hr:11 hr light:dark cycle. The air and
361 water temperature in the zebrafish facility are maintained at 26-28°C. Zebrafish larvae
362 used in experiments (7–9 dpf) were transferred between the facility and the
363 experimental apparatus in zebrafish husbandry system water (H.S.W.) and kept at 26-
364 28°C between experiments.

365

366 **Tg[CAG$_{NRSE}$:GCaMP6s]**

367 To monitor cell Ca^{++} activity in these experiments, we used the transgenic zebrafish
368 Tg[CAG$_{NRSE}$:GCaMP6s] with GCaMP6s (Chen et al., 2013) expression driven by a β-
369 Actin promoter (Quitschke et al., 1989) to drive widespread expression and 3X NRSE
370 (neuron-restrictive silencer element) to restrict expression to neurons (Bergeron et al.,
371 2012).

372

373 **Tg[tiam2a:GFP]**

374 The transgenic fish y264Et (originally created by the lab of Harold Burgess), with the
375 construct Et(SCP1:GAL4FF), uniquely labels Tiam2a-positive cells with GFP within the
376 rostrolateral pallium (Sprague et al., 2003).

377 This transgenic fish was deposited in the ZFIN database (Ruzicka et al., 2015) with the
378 following citation: Marquart, G.D., Tabor, K.M., Brown, M., Strykowski, J.L., Varshney,
379 G.K., LaFave, M.C., Mueller, T., Burgess, S.H., Higashijima, S., and Burgess, H.A.
380 (2015) Enhancer Trap Transgenics. ZFIN Direct Data Submission. (http://zfin.org).

381 **Mounting Zebrafish in Caddie for Imaging on FlexSPIM**

382 To prepare for behavioral experiments, zebrafish subjects were first embedded in a
383 custom behavioral training caddie generated by Protolabs (Stereolithography, ABS-like
384 Translucent Clear [WaterShed]). Specs: ABS-Like Translucent Clear (WaterShed),

385 Normal Res, Natural, Stereolithography, X: 0.980in Y: 0.206in Z: 0.311in. The caddie is
386 filled with 200 mL of 1% (w/v) agarose, melting point ≤ 65°C (Millipore Sigma;
387 SeaPlaque, Cat:50101) dissolved in egg water containing methylene blue, which
388 suppresses fungal growth. During agarose embedding and fluorescence imaging
389 experiments, zebrafish were anesthetized in a final concentration of 70 ppm MS-222
390 (Western Chemical, Fluka analytical, Cat: A5040-100G) + 70 ppm Isoflurane (Phoenix
391 SKU 012ABB-250CC), an IACUC-approved combination that has been shown to enable
392 fast recovery from anesthesia as compared to using MS-222 alone (Huang WC*, et al.,*
393 2010). The anesthetics are dissolved in filter sterilized HSW. For all experiments
394 involving agarose- embedding of the zebrafish, a 1.5% (w/v) solution of low melting
395 point agarose (Sea Plaque Agarose, Lonza) dissolved in filter sterilized husbandry
396 system water consisting of instant ocean (ASIN: B000255NKA) and baking soda
397 dissolved in reverse osmosis water to achieve pH 7.2 and a conductance of ~700 μS)
398 with anesthetic is used. There was no bias in zebrafish sex for larval experiments, as
399 sex determination does not occur in zebrafish before the juvenile stage, ~24 dpf (Uchida
400 et al., 2002).
401
402 As the agarose solidifies (before it completely solidifies at 5 min), a hair stem (human
403 hair attached to a plastic rod) is used to position the zebrafish so that the body axis is
404 parallel to the surface of the chamber (normal swimming orientation). Once the agarose
405 solidifies, the caddie is placed into a 60 mm culture dish (Corning, Cat: 430166) and 10
406 ml of fresh filter-sterilized H.S.W. is added. The agarose is then shaved down with a
407 razor such that only the head and body are encased. Before the anesthetic wears off

408 after the introduction of the fresh H.S.W. solution (~30 seconds), the tail of the zebrafish
409 (just posterior to the swim bladder) is carefully freed from the agarose using fine forceps
410 (biology tip profile, Fine Science Tools, Cat: 11251-10). The rostral aspect of the
411 zebrafish (anterior to the swim bladder) is held firmly in place by the agarose. The
412 caddie is then transferred to another 60 mm culture dish in preparation for
413 transportation to the imaging room.

414 **FlexSPIM Light Sheet Microscope**

415 After the zebrafish has been mounted into the custom Protolabs caddie, it is ready to be
416 placed onto the flexSPIM. The flexSPIM is a versatile, multi-laser twin-microscope
417 system for light-sheet imaging designed and built for multiphoton and visible wavelength
418 fluorescence light sheet excitation (Keomanee-Dizon et al., 2020). The caddie is
419 securely fastened on the dive bar and placed into the chamber filled with 80 ml of fresh,
420 filter-sterilized H.S.W. During imaging, the objective position is programmed to follow a
421 saw waveform such that the objective takes a unidirectional path starting at the top of
422 the fish pallium (0 mm) and transitioning through to the most ventral aspect of pallium
423 (60 mm) at a frequency of 0.75 Hz. The brain camera follows a square waveform that
424 instructs it to acquire 11 images per objective cycle.

425 **Arduino**

426 For the behavioral experiments, an Arduino unit (Arduino UNO Rev3, Arduino.cc) and
427 the software (Arduino software [IDE]) from the same company are used to control the
428 stimuli. For the IR experiments, a simple program was designed to control the infrared
429 laser (NIR RLCO-980-1000-F laser, Roithner Lasertechnik) by turning it on and off for

430 two seconds, every two minutes. For the electricity experiments, a simple program was
431 designed to allow the native Arduino 5V output to be turned on and off for 400 ms every
432 two minutes.

433 **Volumetric Visualization of Neural Activation**

434 To visualize stimulus-evoked neural activation, volumetric calcium-imaging data were
435 reconstructed into three-dimensional heat maps. Eleven consecutive image planes
436 acquired with the flexSPIM immediately before stimulus onset were combined to
437 generate a baseline 3D fluorescence volume. The same procedure was repeated for
438 frames acquired after the stimulus (the specific time selected was within a 3 s post-
439 stimulus window to capture the peak GCaMP response). The pre- and post-stimulus
440 volumes were visualized side-by-side to illustrate regional activation patterns. Each 3D
441 volume was rendered in coronal and dorsal orientations and manually curated to
442 exclude superficial skin layers and non-neuronal regions, providing volumetric heat
443 maps of GCaMP fluorescence before and after stimulation
444

445 **Time-Lapse Analysis of Whole Regions**

446 To quantify the temporal dynamics of stimulus-evoked activity within a region as a
447 whole, time-lapse calcium-imaging data were analyzed from 90 consecutive frames
448 acquired with the flexSPIM, with frame 45 corresponding to stimulus onset. Data from
449 multiple trials were averaged to generate representative activation profiles for the
450 left/right habenula, left/right rostrolateral regions, and left/right ventromedial regions of
451 the brain. Using ImageJ, regions of interest were manually defined, and the mean

fluorescence intensity was measured across all frames, producing time-series traces of average neuronal activity before, during, and after each stimulus.

Calcium Imaging Data Processing and Spatial Registration

Time-series calcium-imaging data were processed using the open-source CaImAn package (Giovannucci *et al.*, 2019) to perform motion correction, signal extraction, and neuronal component identification. Rigid and non-rigid motion correction were applied to minimize motion artifacts and ensure accurate spatial alignment across frames. Following registration, a constrained non-negative matrix factorization (CNMF) model was applied, with key input parameters (e.g., expected neuron diameter, local-correlation threshold, and signal-to-noise cut-offs) empirically optimized to match the imaging resolution and fluorescence dynamics of the dataset. This optimization yielded spatial footprints and corresponding ΔF/F fluorescence traces for individual neuronal components. Model performance was iteratively evaluated through inspection of residual maps and assessment of spatial–temporal consistency.

Neuronal components were selected from anatomically defined regions and depths encompassing the habenula (~10 μm), rostrolateral region (~30 μm), and ventromedial region (~50 μm). Each region consisted of two bilaterally symmetric areas measuring approximately 50 μm × 50 μm. The habenula regions were located at the most caudal aspect of the brain, the rostrolateral regions were positioned rostrally and laterally, and the ventromedial regions were situated ventrally and medially, near the midline of the brain. Within each region, ΔF/F fluorescence traces were extracted for all identified neuronal components.

To correct for gradual fluorescence-intensity drift resulting from photobleaching, a rolling mean filter with a window size of 10 frames was applied to stabilize the ΔF/F time series. For each stimulus type, five trials were performed, except for the partial-looming stimulus, which was presented three times. For every trial, 44 frames preceding (~1min) and 45 frames following (~1min) the stimulus onset were extracted and averaged across trials, with frame 45 corresponding to the time of stimulus delivery. This procedure produced six averaged 90-frame time series per fish, corresponding to left and right hemispheric regions of the habenula, rostrolateral, and ventromedial areas.

To determine which neuronal components exhibited activation or inhibition in response to the stimulus, the mean ΔF/F values from frames 45–50 (post-stimulus window) were compared with the mean of the preceding 40 frames (baseline). Components showing ΔF/F ≥ +50% relative to baseline were classified as activated, while those with ΔF/F ≤ −50% were classified as inhibited.

Binary activation maps, showing activated and inhibited components for all fish and stimulus conditions were then registered onto a canonical template fish (three templates: habenula, rostrolateral, and vetromedial), with activated components represented in red and inhibited components in blue. The canonical template was constructed to represent an "ideal" reference fish and to standardize minor morphological variations across individuals. Registration parameters were manually ascertained using ITK-SNAP, using the midline and the skin-brain boundaries as anatomical landmarks. Using these parameters, each image analyzed was geometrically transformed (cropped, scaled, rotated, and translated) to align with the

496 appropriate canonical template using custom Python scripts incorporating the libraries
497 OpenCV, Matplotlib, and NumPy. The XY coordinates of activated and inhibited
498 components were then extracted from the registered images and plotted onto the
499 canonical template to generate composite activation/inhibition maps showing bilateral
500 regional responses to each stimulus.

501 **Heating Tg[tiam2a:GFP] Larval Zebrafish using an IR Laser (Figure 9)**

502 Experimental procedures in this section were partially adapted from (Dempsey et al.,
503 2022). To begin, Tg[tiam2a:GFP] zebrafish larvae were embedded in custom behavioral
504 training molds: a 60 mm culture dish filled with 1% agarose dissolved in egg water, with
505 a 10 mm diameter circle cut out from the center. The zebrafish was anesthetized and
506 then embedded in the 10 mm diameter circle with 500 ml agarose + anesthetic (70 ppm
507 MS-222 + 70 ppm Isoflurane (SKU 012ABB-250CC). While the agarose solidified, the
508 zebrafish's position was parallel to the surface of the chamber, at the top of the agarose
509 surface, and was maintained using a single bristle brush. After 5 min, 10 mL of sterilized
510 husbandry system water was added to the chamber. Using fine forceps, the tail of the
511 zebrafish was carefully freed from the agarose. All free-floating agarose was removed
512 from the dish. The dish was then positioned under the objective of a custom-built
513 behavioral microscope such that the right eye of the zebrafish was directly under where
514 the infrared laser spot would be when turned on (NIR RLCO-980-1000-F laser, Roithner
515 Lasertechnik). An Arduino was programmed to deliver the infrared heating laser for two
516 seconds, a total of ten times, with an intertrial separation of 2 minutes. After the fish
517 underwent ten trials, it was then fixed in PFA prior to pERK immunohistochemistry.

518

519 **pERK Immunohistochemistry**

520 After exposing 7–9 dpf Tg[tiam2a;GFP] larval zebrafish to the infrared laser ten times,
521 zebrafish were fixed in 4% PFA diluted in 1x PBS (pH 7.4), 70 ppm MS-222, 70 ppm
522 Isoflurane, covered in aluminum foil, and kept at 4°C overnight. Then, fish were washed
523 3 times in 1x PBS (pH 7.4) and 0.25% PBST (0.25% Triton X-100 in PBS). After 3x
524 PBST washes, the zebrafish were placed in 150 mM Tris HCl (pH 9) for 5 min at room
525 temperature, followed by 20 minutes at 65°C. Once this was complete, the samples
526 were cooled to room temperature and given 3x PBST washes. Zebrafish were then
527 permeabilized on ice for 45 minutes with 1x PBS, 0.05% Trypsin-EDTA (Sigma, T4049-
528 100ML) diluted in 1x PBS (pH 7.4). After another 3x PBST wash cycle, the zebrafish
529 were placed for 1 hour at room temperature in blocking buffer solution; (1x PBS, 1%
530 bovine serum albumin, 2% DMSO, 2% NGS, 0.25% Triton X-100. Zebrafish were
531 stained with primary rabbit anti-phosphorylated Erk1/2 antibodies at a 1:300 dilution
532 (Cell Signaling, Catalog #4696) in blocking buffer on a rotating platform at 4°C
533 overnight. After 5X PBST washes, the zebrafish were transferred to a blocking buffer
534 solution containing a 1:1000 dilution of Alexa Fluor 568-conjugated goat anti-rabbit
535 secondary antibody (Invitrogen, A-11011) and incubated overnight at 4°C on an orbital
536 shaker in the dark. After 5 PBST washes, samples were moved to PBS solution and
537 imaged on a Zeiss LSM 780 confocal (Translational Imaging Center, USC).

538

539 **Statistical Analysis**

540 Calcium signal curves and heatmaps were calculated using Python 3.12 scripts.
541 Statistical differences for pre- vs post-stimulus AUC values were assessed using one-
542 tailed paired t-tests implemented in the SciPy library, and $p < 0.05$ was considered
543 statistically significant. No statistical methods were used to predetermine sample size.

544 **Experimental Setup and Stimulation Protocols for Neuronal Activity Imaging in**
545 **Fish**

546 All fish used in this study were given 90 min to acclimate on the flexSPIM system.
547 Following acclimation, each fish was imaged for 5 min to establish a baseline for
548 neuronal activity before being exposed to stimuli. The total duration of the experiments
549 was ~15-20 min. After the experiment was finished, the fish was released from the
550 agarose and allowed to rest in a dish for one hour. Only fish that were still alive and
551 healthy after this waiting time were included in the analysis.
552

553 **Near-Infrared laser**

554 Once the fish was prepared for imaging, it was positioned such that its right eye was hit
555 by the IR laser (NIR RLCO-980-1000-F laser, Roithner Lasertechnik). While imaging,
556 the IR laser was turned on for 2 seconds before being turned off. This was repeated 2
557 minutes later for a total of 5 trials.

558 **Electric shock**

559 Once the fish was prepared for imaging, two 1-pin dual-male jumper wires were
560 secured onto the dive bar such that the pin connectors were positioned on or near both

sides of the fish, where the body meets the tail. They were positioned such that when current is applied, it travels between the wires, creating a circuit with the fish in between, causing a small electric shock. While imaging, a 500 mA electric shock was administered to the zebrafish through electrodes connected to a 5 V Arduino pin for 400 ms. This was repeated every 2 minutes, for a total of 5 trials.

Full-looming Stimulus

Once the fish was prepped for imaging, a red-backlit projector screen was positioned on the right side of the fish. The window on the chamber covered 66° of the fish's visual field. A small black circle (1° of the fish's visual field) was maintained throughout the duration of the experiment. At the beginning of each trial, the spot was expanded until it fully covered the entire projection screen (1° to 66 degrees of the visual field) over 500 ms, hence the name "full-looming stimulus". Following 5 s, the stimulus returned to its original size. This was repeated 2 min later for a total of 5 trials.

Partial-looming stimulus

Once the fish was prepped for imaging, it was exposed to a stimulus similar to the full-looming stimulus, except that the black circle expanded to 48° over 300 ms, partially covering the visual field. The black circle remained at 48° for 5 seconds before contracting back to its original size of 1° over 300 ms. This process was repeated 2 min later, for a total of 3 trials.

Tapping

During imaging, the experimenter tapped the side of the chamber with a plastic stick for 5 s. This process was repeated 2 min later, for a total of 5 trials.

Airhorn

While imaging, an air horn (1.4 oz, Betterboat) sounded a 120-130 dB blast approximately 1 inch above the chamber. The experimenter wore ear protection to prevent hearing damage. This procedure was repeated 2 minutes later, for a total of 5 trials.

Light

Once the fish was prepared for imaging, a red-backlit projector screen was positioned on the right side of the fish, making the light visible to the fish. A small, removable cardboard card was then placed between the fish and the projector, keeping the fish in complete darkness. During imaging, the card was removed for 5 s to expose the fish to light. After 5 seconds, the card was placed back between the fish and the projector to block the light. This procedure was repeated 2 minutes later, for a total of 5 trials.

Data Availability

Raw and processed data on Jupyter notebooks containing analysis pipelines are available on https://gin.g-node.org/coltonsm/Zebrafish_Valence_Project**.** The DOI for this repository will be made public upon being accepted for publication.

606 **Acknowledgements**

607 We thank M. Jones for microscopy technical support in the Translational Imaging
608 Center, K. Keomanee-Dizon for the design and construction of the SPIM setup, and L.
609 Trinh and E. Carranza Lopez for zebrafish husbandry support. All microscopy was done
610 at the Translational Imaging Center. This work was supported by the National Institute
611 of Mental Health Grant 1UF1NS122082.

612

613 **References**

614 Ahrens MB, Orger MB, Robson DN, Li JM, Keller PJ. 2013. Whole-brain functional
615 imaging at cellular resolution using light-sheet microscopy. Nat Methods
616 10:413–420. DOI: https://doi.org/10.1038/nmeth.2434, PMID: 23524393
617 Baker MR, Wong RY. 2021. Npas4a expression in the teleost forebrain is
618 associated with stress coping style differences in fear learning. Scientific
619 Reports 11. DOI: https://doi.org/10.1038/s41598-021-91495-7, PMID:
620 34103598
621 Bartoszek EM, Ostenrath AM, Jetti SK, Serneels B, Mutlu AK, Chau KTP, Yaksi E.
622 2021. Ongoing habenular activity is driven by forebrain networks and
623 modulated by olfactory stimuli. Curr Biol 31:3861-3874 e3. DOI:
624 https://doi.org/10.1016/j.cub.2021.08.021, PMID: 34416179
625 Bechara A, Damasio H, Damasio AR. 2003. Role of the amygdala in decision-
626 making. Ann N Y Acad Sci 985:356–369. DOI: https://doi.org/10.1111/j.1749-
627 6632.2003.tb07094.x, PMID: 12724171
628 Belova MA, Paton JJ, Salzman CD. 2008. Moment-to-moment tracking of state
629 value in the amygdala. Journal of Neuroscience 28:10023–10030. DOI:
630 https://doi.org/10.1523/JNEUROSCI.1400-08.2008, PMID: 18829960
631 Beppi C, Beringer G, Straumann D, Bogli SY. 2021. Light-stimulus intensity
632 modulates startle reflex habituation in larval zebrafish. Sci Rep 11:22410. DOI:
633 https://doi.org/10.1038/s41598-021-00535-9, PMID: 34789729
634 Bergeron SA, Hannan MC, Codore H, Fero K, Li GH, Moak Z, Yokogawa T,
635 Burgess HA. 2012. Brain selective transgene expression in zebrafish using an
636 NRSE derived motif. Front Neural Circuits 6:110. DOI:
637 https://doi.org/10.3389/fncir.2012.00110, PMID: 23293587
638 Beyeler A, Chang CJ, Silvestre M, Leveque C, Namburi P, Wildes CP, Tye KM.
639 2018. Organization of Valence-Encoding and Projection-Defined Neurons in

640 the Basolateral Amygdala. Cell Rep 22:905–918. DOI:
641 https://doi.org/10.1016/j.celrep.2017.12.097, PMID: 29386133
642 Broglio C, Gomez A, Duran E, Ocana FM, Jimenez-Moya F, Rodriguez F, Salas C.
643 2005. Hallmarks of a common forebrain vertebrate plan: specialized pallial
644 areas for spatial, temporal and emotional memory in actinopterygian fish. Brain
645 Res Bull 66:277–281. DOI: https://doi.org/10.1016/j.brainresbull.2005.03.021,
646 PMID: 16144602
647 Chen TW, Wardill TJ, Sun Y, Pulver SR, Renninger SL, Baohan A, Schreiter ER,
648 Kerr RA, Orger MB, Jayaraman V, Looger LL, Svoboda K, Kim DS. 2013.
649 Ultrasensitive fluorescent proteins for imaging neuronal activity. Nature
650 499:295–300. DOI: https://doi.org/10.1038/nature12354, PMID: 23868258
651 Chiu C-Y, Leng S, Martin KA, Kim E, Gorman S, Duhl DMJ. 1999. Cloning and
652 Characterization of T-Cell Lymphoma Invasion and Metastasis 2 (TIAM2), a
653 Novel Guanine Nucleotide Exchange Factor Related to TIAM1.
654 Clem RL, Huganir RL. 2010. Calcium-permeable AMPA receptor dynamics mediate
655 fear memory erasure. Science 330:1108–1112. DOI:
656 https://doi.org/10.1126/science.1195298, PMID: 21030604
657 Corder G, Ahanonu B, Grewe BF, Wang D, Schnitzer MJ, Scherrer G. 2019. An
658 amygdalar neural ensemble that encodes the unpleasantness of pain. Science
659 363:276–281. DOI: https://doi.org/10.1126/science.aap8586
660 Dempsey WP, Du Z, Nadtochiy A, Smith CD, Czajkowski K, Andreev A, Robson
661 DN, Li JM, Applebaum S, Truong T V, Kesselman C, Fraser SE, Arnold DB.
662 2022. Regional synapse gain and loss accompany memory formation in larval
663 zebrafish. Proc Natl Acad Sci U S A 119. DOI:
664 https://doi.org/10.1073/pnas.2107661119, PMID: 35031564
665 Downer DJLD. 1961. CHANGES IN VISUAL GNOSTIC FUNCTIONS AND
666 EMOTIONAL BEHAVIOUR FOLLOWING UNILATERAL TEMPORAL POLE
667 DAMAGE IN THE “SPLIT-BRAIN” MONKEY. *NATURE*.
668 Eaton RC, Lee RK, Foreman MB. 2001. The Mauthner cell and other identified
669 neurons of the brainstem escape network of fish. Prog Neurobiol 63:467–485.
670 DOI: https://doi.org/10.1016/s0301-0082(00)00047-2, PMID: 11163687
671 Fadok JP, Krabbe S, Markovic M, Courtin J, Xu C, Massi L, Botta P, Bylund K,
672 Müller C, Kovacevic A, Tovote P, Lüthi A. 2017. A competitive inhibitory circuit
673 for selection of active and passive fear responses. Nature 542:96–99. DOI:
674 https://doi.org/10.1038/nature21047, PMID: 28117439
675 Feinstein JS, Adolphs R, Damasio A, Tranel D. 2011. The human amygdala and
676 the induction and experience of fear. Current Biology 21:34–38. DOI:
677 https://doi.org/10.1016/j.cub.2010.11.042, PMID: 21167712

678 Gerlai R. 2011. Associative Learning in Zebrafish (Danio rerio). *Methods in Cell*
679 *Biology*. DOI: https://doi.org/10.1016/B978-0-12-387036-0.00012-8, PMID:
680 21550448
681 Giovannucci A, Friedrich J, Gunn P, Kalfon J, Brown BL, Koay SA, Taxidis J, Najafi
682 F, Gauthier JL, Zhou PC, Khakh BS, Tank DW, Chklovskii DB, Pnevmatikakis
683 EA. 2019. CaImAn an open source tool for scalable calcium imaging data
684 analysis. Elife 8. PMID: WOS:000455875300001
685 Goosens KA, Maren S. 2002. Long-term potentiation as a substrate for memory:
686 evidence from studies of amygdaloid plasticity and Pavlovian fear conditioning.
687 Hippocampus 12:592–599. DOI: https://doi.org/10.1002/hipo.10099, PMID:
688 12440575
689 Grewe BF, Grundemann J, Kitch LJ, Lecoq JA, Parker JG, Marshall JD, Larkin MC,
690 Jercog PE, Grenier F, Li JZ, Luthi A, Schnitzer MJ. 2017. Neural ensemble
691 dynamics underlying a long-term associative memory. Nature 543:670–675.
692 DOI: https://doi.org/10.1038/nature21682, PMID: 28329757
693 Herberholz J, Marquart GD. 2012. Decision Making and Behavioral Choice during
694 Predator Avoidance. Front Neurosci 6:125. DOI:
695 https://doi.org/10.3389/fnins.2012.00125, PMID: 22973187
696 Kenney JW, Scott IC, Josselyn SA, Frankland PW. 2017. Contextual fear
697 conditioning in zebrafish. Learn Mem 24:516–523. DOI:
698 https://doi.org/10.1101/lm.045690.117, PMID: 28916626
699 Keomanee-Dizon K, Fraser SE, Truong T V. 2020. A versatile, multi-laser twin-
700 microscope system for light-sheet imaging. Review of Scientific Instruments
701 91. PMID: WOS:000537881400001
702 Kunst M, Laurell E, Mokayes N, Kramer A, Kubo F, Fernandes AM, Forster D, Dal
703 Maschio M, Baier H. 2019. A Cellular-Resolution Atlas of the Larval Zebrafish
704 Brain. Neuron 103:21-38 e5. DOI:
705 https://doi.org/10.1016/j.neuron.2019.04.034, PMID: 31147152
706 Lal P, Tanabe H, Suster ML, Ailani D, Kotani Y, Muto A, Itoh M, Iwasaki M, Wada
707 H, Yaksi E, Kawakami K. 2018. Identification of a neuronal population in the
708 telencephalon essential for fear conditioning in zebrafish. BMC Biol 16:45.
709 DOI: https://doi.org/10.1186/s12915-018-0502-y, PMID: 29690872
710 LeDoux JE, Iwata J, Cicchetti P, Reis DJ. 1988. Different projections of the central
711 amygdaloid nucleus mediate autonomic and behavioral correlates of
712 conditioned fear. J Neurosci 8:2517–2529. PMID: 2854842
713 Manuel R, Gorissen M, Piza Roca C, Zethof J, Van De Vis H, Flik G, Van Den Bos
714 R. 2014. Inhibitory avoidance learning in zebrafish (Danio Rerio): Effects of
715 shock intensity and unraveling differences in task performance. Zebrafish
716 11:341–352. DOI: https://doi.org/10.1089/zeb.2013.0970, PMID: 25004302

Mueller T, Dong Z, Berberoglu MA, Guo S. 2011. The dorsal pallium in zebrafish, Danio rerio (Cyprinidae, Teleostei). Brain Res 1381:95–105. DOI: https://doi.org/10.1016/j.brainres.2010.12.089, PMID: 21219890

Nabavi S, Fox R, Proulx CD, Lin JY, Tsien RY, Malinow R. 2014. Engineering a memory with LTD and LTP. Nature 511:348–352. DOI: https://doi.org/10.1038/nature13294, PMID: 24896183

Namburi P, Beyeler A, Yorozu S, Calhoon GG, Halbert SA, Wichmann R, Holden SS, Mertens KL, Anahtar M, Felix-Ortiz AC, Wickersham IR, Gray JM, Tye KM. 2015. A circuit mechanism for differentiating positive and negative associations. Nature 520:675–678. DOI: https://doi.org/10.1038/nature14366, PMID: 25925480

Neo YY, Parie L, Bakker F, Snelderwaard P, Tudorache C, Schaaf M, Slabbekoorn H. 2015. Behavioral changes in response to sound exposure and no spatial avoidance of noisy conditions in captive zebrafish. Front Behav Neurosci 9:28. DOI: https://doi.org/10.3389/fnbeh.2015.00028, PMID: 25741256

Olszewski J, Haehnel M, Taguchi M, Liao JC. 2012. Zebrafish larvae exhibit rheotaxis and can escape a continuous suction source using their lateral line. PLoS ONE 7. DOI: https://doi.org/10.1371/journal.pone.0036661, PMID: 22570735

Penzo MA, Robert V, Li B. 2014. Fear conditioning potentiates synaptic transmission onto long-range projection neurons in the lateral subdivision of central amygdala. Journal of Neuroscience 34:2432–2437. DOI: https://doi.org/10.1523/JNEUROSCI.4166-13.2014, PMID: 24523533

Phillips RG, LeDoux JE. 1992. Differential contribution of amygdala and hippocampus to cued and contextual fear conditioning. Behav Neurosci 106:274–285. PMID: 1590953

Portavella M, Torres B, Salas C. 2004. Avoidance response in goldfish: emotional and temporal involvement of medial and lateral telencephalic pallium. J Neurosci 24:2335–2342. DOI: https://doi.org/10.1523/JNEUROSCI.4930-03.2004, PMID: 14999085

Portavella Manuel, Torres B, Salas C. 2004. Avoidance Response in Goldfish: Emotional and Temporal Involvement of Medial and Lateral Telencephalic Pallium. Journal of Neuroscience 24:2335–2342. DOI: https://doi.org/10.1523/JNEUROSCI.4930-03.2004, PMID: 14999085

Portavella M, Vargas JP, Torres B, Salas C. 2002. The effects of telencephalic pallial lesions on spatial, temporal, and emotional learning in goldfish. Brain Res Bull 57:397–399. PMID: 11922997

Quirk GJ, Repa C, LeDoux JE. 1995. Fear conditioning enhances short-latency auditory responses of lateral amygdala neurons: parallel recordings in the freely behaving rat. Neuron 15:1029–1039. PMID: 7576647

757 Quitschke WW, Lin ZY, DePonti-Zilli L, Paterson BM. 1989. The β actin promoter.
758 Journal of Biological Chemistry 264:9539–9546. DOI:
759 https://doi.org/10.1016/s0021-9258(18)60565-4
760 Rogan MT, Staubli U V, LeDoux JE. 1997. Fear conditioning induces associative
761 long-term potentiation in the amygdala. Nature 390:604–607. DOI:
762 https://doi.org/10.1038/37601, PMID: 9403688
763 Ruhl T, Moesbauer K, Oellers N, von der Emde G. 2015. The endocannabinoid
764 system and associative learning and memory in zebrafish. Behavioural Brain
765 Research 290:61–69. DOI: https://doi.org/10.1016/j.bbr.2015.04.046, PMID:
766 25956869
767 Ruzicka L, Bradford YM, Frazer K, Howe DG, Paddock H, Ramachandran S,
768 Singer A, Toro S, Van Slyke CE, Eagle AE, Fashena D, Kalita P, Knight J,
769 Mani P, Martin R, Moxon SAT, Pich C, Schaper K, Shao X, Westerfield M.
770 2015. ZFIN, The zebrafish model organism database: Updates and new
771 directions. Genesis 53:498–509. DOI: https://doi.org/10.1002/dvg.22868,
772 PMID: 26097180
773 Smith DM, Torregrossa MM. 2021. Valence encoding in the amygdala influences
774 motivated behavior. *Behavioural Brain Research*. DOI:
775 https://doi.org/10.1016/j.bbr.2021.113370, PMID: 34051230
776 Sprague J, Clements D, Conlin T, Edwards P, Frazer K, Schaper K, Segerdell E,
777 Song P, Sprunger B, Westerfield M. 2003. The Zebrafish Information Network
778 (ZFIN): The zebrafish model organism database. *Nucleic Acids Research*.
779 DOI: https://doi.org/10.1093/nar/gkg027, PMID: 12519991
780 Temizer I, Donovan JC, Baier H, Semmelhack JL. 2015. A Visual Pathway for
781 Looming-Evoked Escape in Larval Zebrafish. Curr Biol 25:1823–1834. DOI:
782 https://doi.org/10.1016/j.cub.2015.06.002, PMID: 26119746
783 Truong T V, Supatto W, Koos DS, Choi JM, Fraser SE. 2011. Deep and fast live
784 imaging with two-photon scanned light-sheet microscopy. Nat Methods 8:757–
785 760. DOI: https://doi.org/10.1038/nmeth.1652, PMID: 21765409
786 Tye KM. 2018. Neural Circuit Motifs in Valence Processing. *Neuron*. DOI:
787 https://doi.org/10.1016/j.neuron.2018.10.001, PMID: 30359607
788 Tye KM, Prakash R, Kim SY, Fenno LE, Grosenick L, Zarabi H, Thompson KR,
789 Gradinaru V, Ramakrishnan C, Deisseroth K. 2011. Amygdala circuitry
790 mediating reversible and bidirectional control of anxiety. Nature 471:358–362.
791 DOI: https://doi.org/10.1038/nature09820, PMID: 21389985
792 Uchida D, Yamashita M, Kitano T, Iguchi T. 2002. Oocyte apoptosis during the
793 transition from ovary-like tissue to testes during sex differentiation of juvenile
794 zebrafish. J Exp Biol 205:711–718. PMID: 11914381
795 Vladimirov N, Wang C, Höckendorf B, Pujala A, Tanimoto M, Mu Y, Yang CT,
796 Wittenbach JD, Freeman J, Preibisch S, Koyama M, Keller PJ, Ahrens MB.

797 2018. Brain-wide circuit interrogation at the cellular level guided by online
798 analysis of neuronal function. Nature Methods 15:1117–1125. DOI:
799 https://doi.org/10.1038/s41592-018-0221-x, PMID: 30504888
800 von Trotha JW, Vernier P, Bally-Cuif L. 2014. Emotions and motivated behavior
801 converge on an amygdala-like structure in the zebrafish. European Journal of
802 Neuroscience 40:3302–3315. DOI: https://doi.org/10.1111/ejn.12692, PMID:
803 25145867
804 Xiu J, Zhang Q, Zhou T, Zhou TT, Chen Y, Hu H. 2014. Visualizing an emotional
805 valence map in the limbic forebrain by TAI-FISH. Nature Neuroscience
806 17:1552–1559. DOI: https://doi.org/10.1038/nn.3813, PMID: 25242305
807 Zhang X, Li B. 2018. Population coding of valence in the basolateral amygdala.
808 Nature Communications 9. DOI: https://doi.org/10.1038/s41467-018-07679-9,
809 PMID: 30518754
810

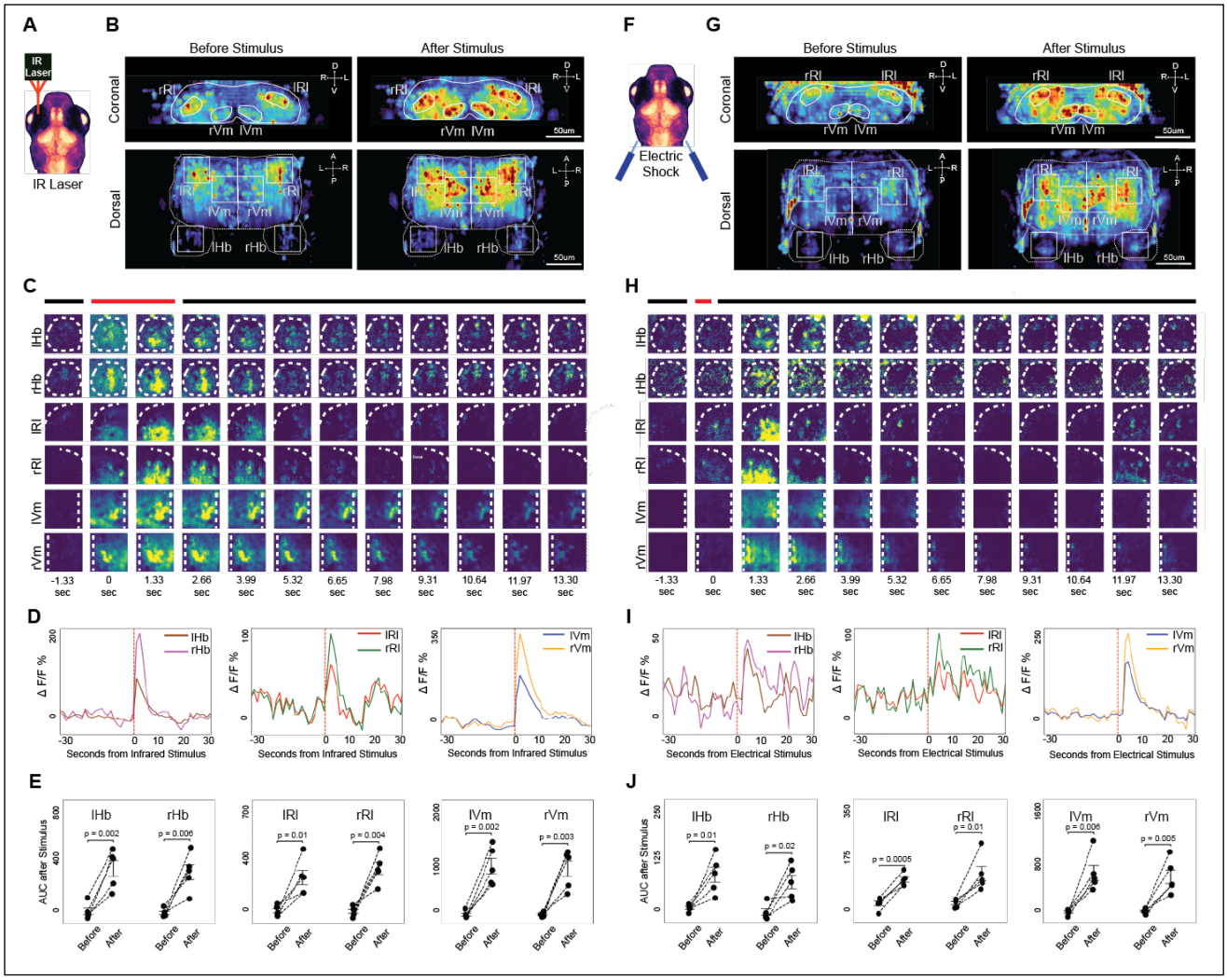

Figure 1 Neuronal activation in response to IR heating and electric shock

(**A**) Experimental setup with an infrared (IR) laser aimed at a 7 dpf larval zebrafish to deliver a heat stimulus.

(**B**) Heat maps of GCaMP fluorescence from a representative fish averaged over 5 presentations of IR heating. Enhanced activity is displayed in rostrolateral (lRL, rRL) and ventromedial (lVm, rVm) areas of the pallium, and habenula (lHb, rHb) in coronal and dorsal views post-laser exposure.

(**C**) Timelapse of average neuronal activation in response to exposure to the IR laser in the forebrain of a representative zebrafish. Each square corresponds to an area outlined in the dorsal view in (B). Brain regions where activity measurements were taken are outlined with dotted lines. Background activity was subtracted from all images.

(**D**) Region-specific ΔF/F activity traces from a representative fish, averaged across 5 trials, display pronounced increases in all measured areas following IR laser exposure.

(**E**) Analysis of the area under the curve (AUC; 5 frames, 6.65 seconds) ΔF/F for each fish for each brain region outlined in (**B**, **C**). Mean ± SEM for n=5 fish.

(**F**) Illustration of electric shock delivery to a 7 dpf larval zebrafish.

(**G**) Heat maps from a representative fish averaged over 5 presentations of electric shock. Enhanced activity is displayed in rostrolateral (lRL, rRL) and ventromedial (lVm, rVm) areas of the pallium, and habenula (lHb, rHb) in coronal and dorsal views post-laser exposure.

(**H**) Timelapse of average neuronal activation in response to exposure to electric shock in the forebrain of a representative zebrafish. Each square corresponds to an area outlined in the dorsal view in (G). Brain regions where activity measurements were taken are outlined with dotted lines. Background activity was subtracted from all images.

(**I**) Region-specific ΔF/F activity traces from a representative fish, averaged across 5 trials, display pronounced increases in all measured areas following electric shock.

(**J**) Analysis of the area under the curve (AUC; 4 frames, 5.32 seconds) ΔF/F for each fish for each brain region outlined in (G, H). Mean ± SEM for n=5 fish.

One-way t-test was used for all statistical comparisons.

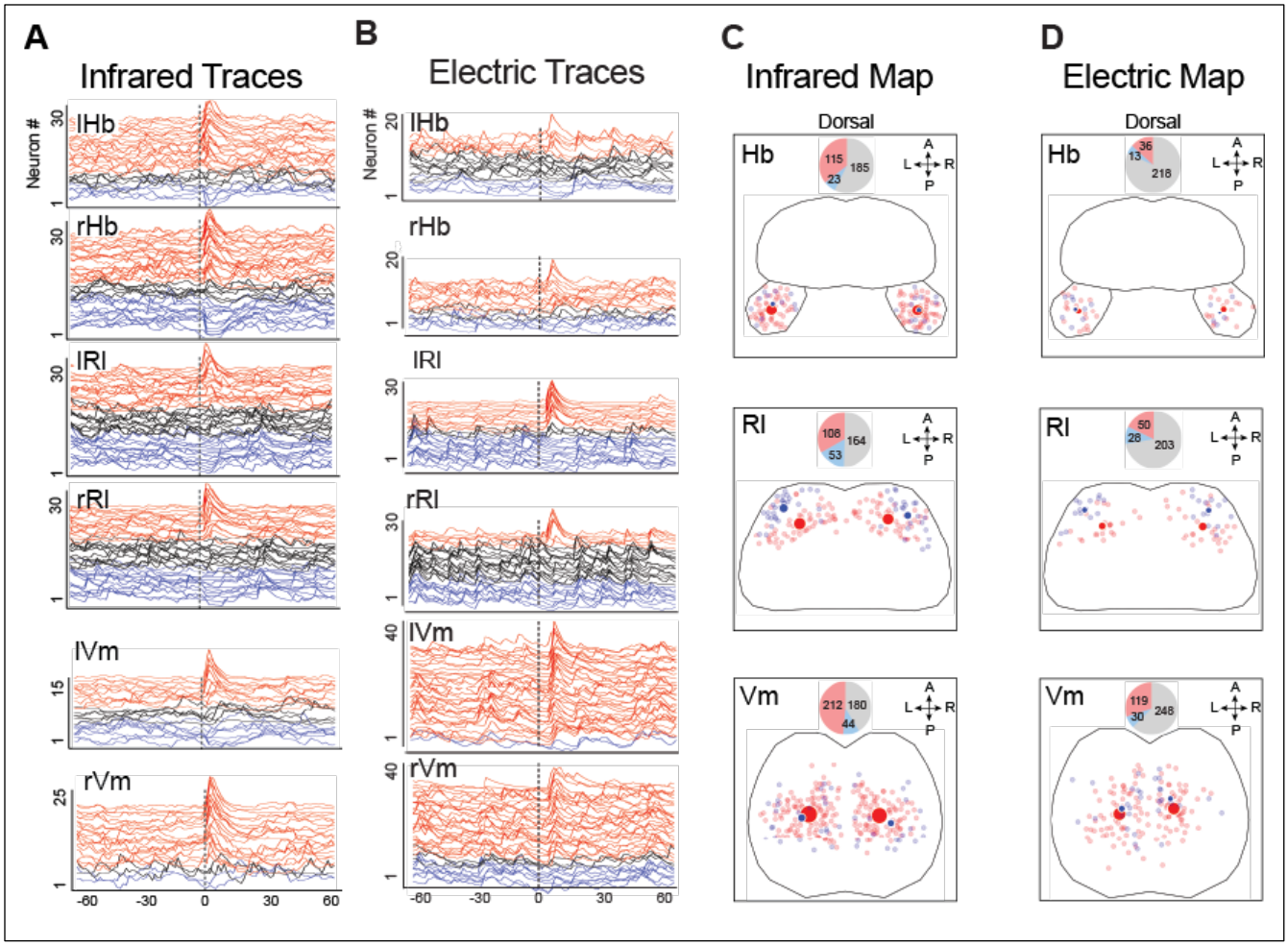

Figure 2. Response of neuronal components to noxious heat stimuli and electric shock.

(A) Neuronal component ΔF/F traces from an example fish as determined by CaImAn reveal a diverse response upon IR stimulation at the vertical dotted line. Red denotes activation (increase in activity ≥ 50% of background DF/F); blue, inhibition (decrease in activity ≤ -50% of background DF/F); Black, neither. Order is determined by z-score (μ/σ), which is a measure of the magnitude and consistency of the response.

(**B**) Neuronal component ΔF/F traces as in (A) in response to electric shock at the vertical dotted line.

(**C**) Locations of activated (small red dots) and inhibited (small blue dots) neuronal components in response to heating with an IR laser for all fish tested. Large dots are centers of mass of corresponding neuronal components. Pie graphs (inset) show the number of activated (red) inhibited (blue), and unresponsive (grey) neuronal components.

(**D**) Same as (C), but for neurons that respond to electric shock

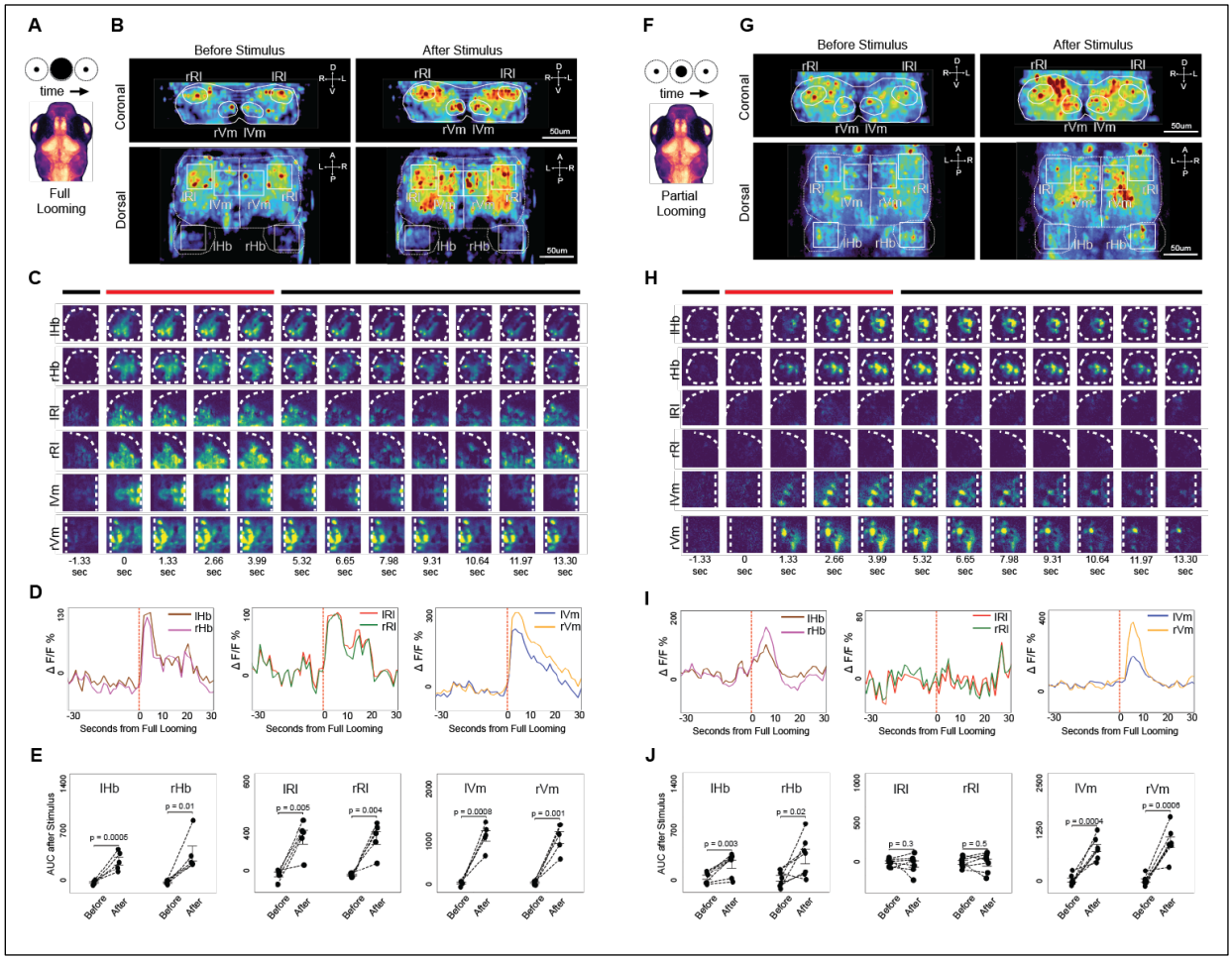

Figure 3. Neuronal activation in response to full and partial looming stimuli.

(**A**) Schematic of a 7 dpf zebrafish subjected to a full-looming disc stimulus.

(**B**) Neuronal activation in a representative zebrafish immediately before and after a full looming stimulus, averaged over 5 presentations, shows an increase in average activity across all brain areas previously found to be activated by noxious stimuli (rHb, lHb, rRl, lRl, rVm, lVm).

(**C**) Timelapse of heatmaps for the six areas outlined in (B) shows an abrupt increase in activity that commences with the full-looming stimulus.

(**D**) Region-specific ΔF/F activity traces from a representative fish, averaged across 5 trials, display pronounced increases in all measured areas following IR laser exposure.

(**E**) Mean increase above background ± SEM for ΔF/F A.U.C. for 5 frames, 6.65 seconds for each fish for each brain region outlined in (B)

(**F**) Schematic of a 7 dpf zebrafish subjected to a partial-looming disc stimulus.

(**G**) Neuronal activation in a representative zebrafish immediately before and after a partial looming stimulus, averaged over 3 presentations.

(**H**) Time-lapse of heatmaps for the six areas outlined in (B) shows an increase in activity in the Hb and Vm regions, but no significant change in activity in the Rl region. Activity in Hb and Vm was sustained for over 10 seconds.

(**I**) Region-specific ΔF/F and activity traces from a representative fish, averaged across 3 trials, display significant activity increases in Hb and Vm, but not in Rl, in response to the partial looming stimulus.

(**J**) Mean increase above background ± SEM for ΔF/F after the partial-looming stimulus (12 frames, ~16 seconds).

All statistical comparisons made with one-way t-test.

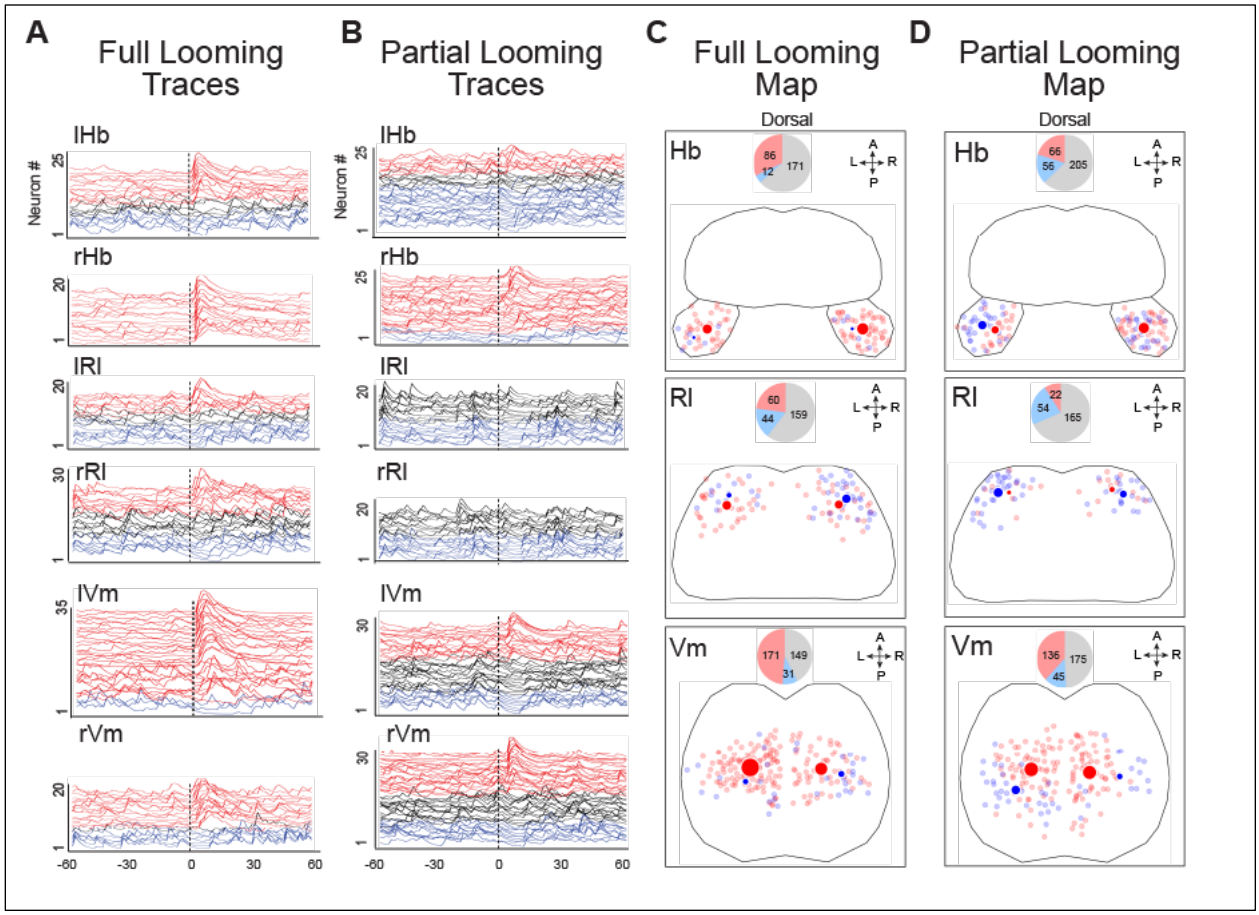

Figure 4. Response of neuronal components to full and partial looming stimuli.

(**A**) Neuronal component ΔF/F traces for an exemplary fish in response to a full looming stimulus at the vertical dotted line, averaged over 5 presentations. Red denotes activation (increase in activity ≥ 50% of background ΔF/F); blue, inhibition (decrease in activity ≤ -50% of background ΔF/F); black, neither. Order is determined by z-score (μ/σ), which is a measure of the magnitude and consistency of the response.

(**B**) Neuronal activity as in (A) in response to a partial looming stimulus averaged over 3 presentations in an exemplary fish. Activated and inhibited traces are seen in Hb and Vm, but not in Rl.

(**C**) Locations of neurons that are activated (small red dots) and inhibited (small blue dots) in response to a full looming stimulus for all fish tested. Large dots are centers of mass of corresponding neuronal components. Pie graphs (inset) show the number of activated (red), inhibited (blue), and unresponsive (grey) neuronal components.

(**D**) Same as (C) in response to a partial looming stimulus for all fish tested.

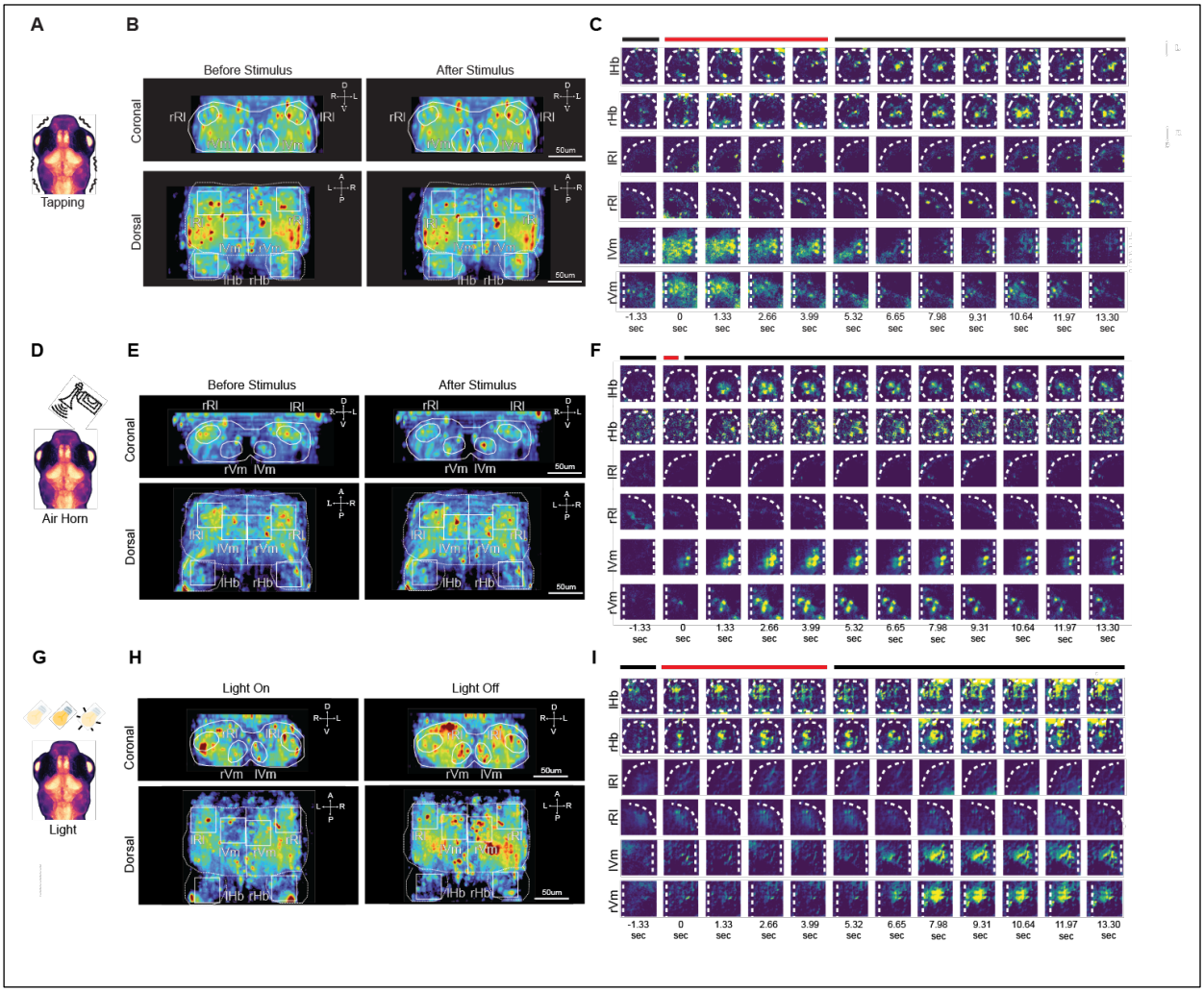

Figure 5. Neuronal activation in response to vibration, a loud noise, and light.

(**A**) Schematic of a 7 dpf zebrafish subjected to vibration.

(**B**) Neuronal activation in a representative zebrafish immediately before and after a vibration stimulus, averaged over 5 presentations, shows an increase in average activity across Hb and Vm, but not RI.

(**C**) Timelapse of heatmaps for areas outlined in (B) show an increase in activity that commences with the initiation of tapping and grows until 14 s after cessation of tapping in Hb. In Vm the activity increases during the tapping stimulus and decreases abruptly after cessation. There is no increase in activity in RI.

(**D**) Schematic of a 7 dpf zebrafish subjected to the blast of an air horn.

(**E**) Neuronal activation in a representative zebrafish immediately before and after an air horn blast, averaged over 5 presentations, shows an increase in average activity across Hb and Vm, but not RI.

(**F**) Timelapse of heatmaps for areas outlined in (E) show an increase in activity that commences with the onset of the loud noise in Hb and Vm and lasts for over 10 s. There is no increase in activity in RI.

(**G**) Schematic of a 7 dpf zebrafish that is first equilibrated to darkness, then exposed to light for 4 s and then returned to darkness.

(**H**) Neuronal activation in a representative zebrafish immediately before and after transitioning from light to darkness, averaged over 5 presentations shows an increase in average activity across Hb and Vm, but not RI.

(**I**) Timelapse of heatmaps for areas outlined in (H) shows an increase in activity in Hb and Vm that commences ~ 2 s after the onset of darkness and lasts for over 5 s. There is no increase in activity in RI.

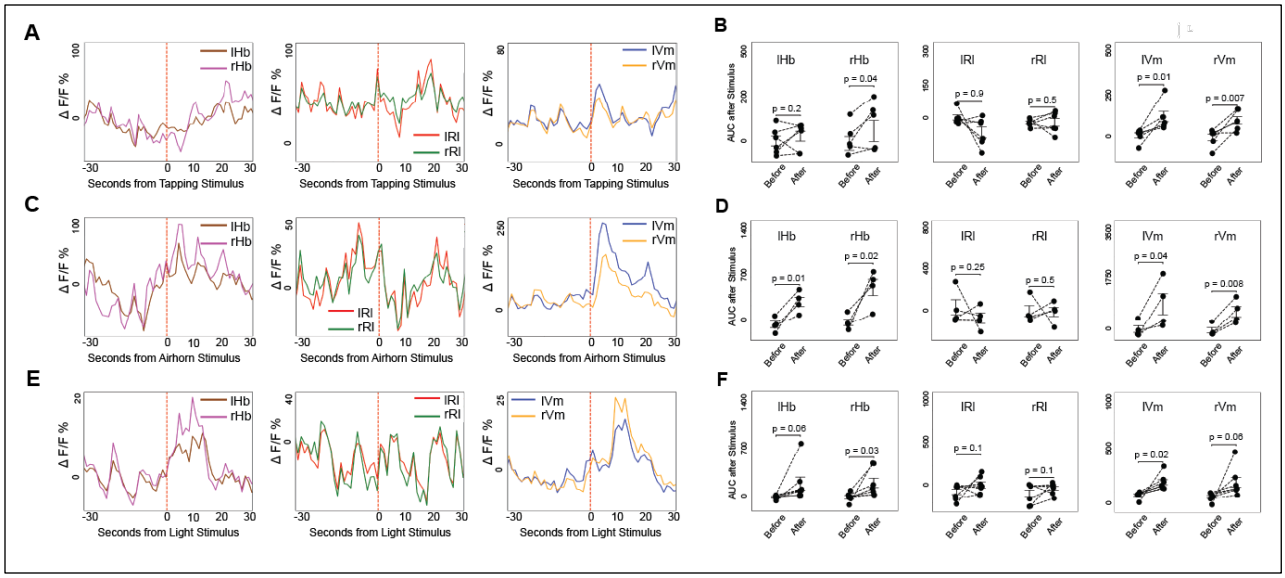

Figure 6 Response of total ΔF/F within different regions to vibration, a loud noise, and light

(**A**) Average ΔF/F activity traces within specific regions from a representative fish, averaged across 5 trials in response to a tapping stimulus.

(**B**) Activity rates for 6 fish before and after the tapping stimulus. Significant increases in activity were seen in rHb, lVm, and rVm, but not in lHb and Rl.

(**C**) Average ΔF/F activity traces within specific regions (AUC; 7 frames, 9.31 seconds) from a representative fish, averaged across 5 trials in response to a blast from an airhorn.

(**D**) Responses to a blast from an airhorn from 4 fish. Significant increases in activity were seen in HB and Vm, but not in Rl.

(**E**) Average ΔF/F activity traces within specific regions from a representative fish, averaged across 5 trials in response to a light-to-dark transition.

(**F**) Responses to a light-to-dark transition from 6 fish. Significant increases in activity were seen in rHB and lVm, but not in lHb, rVm, and Rl.

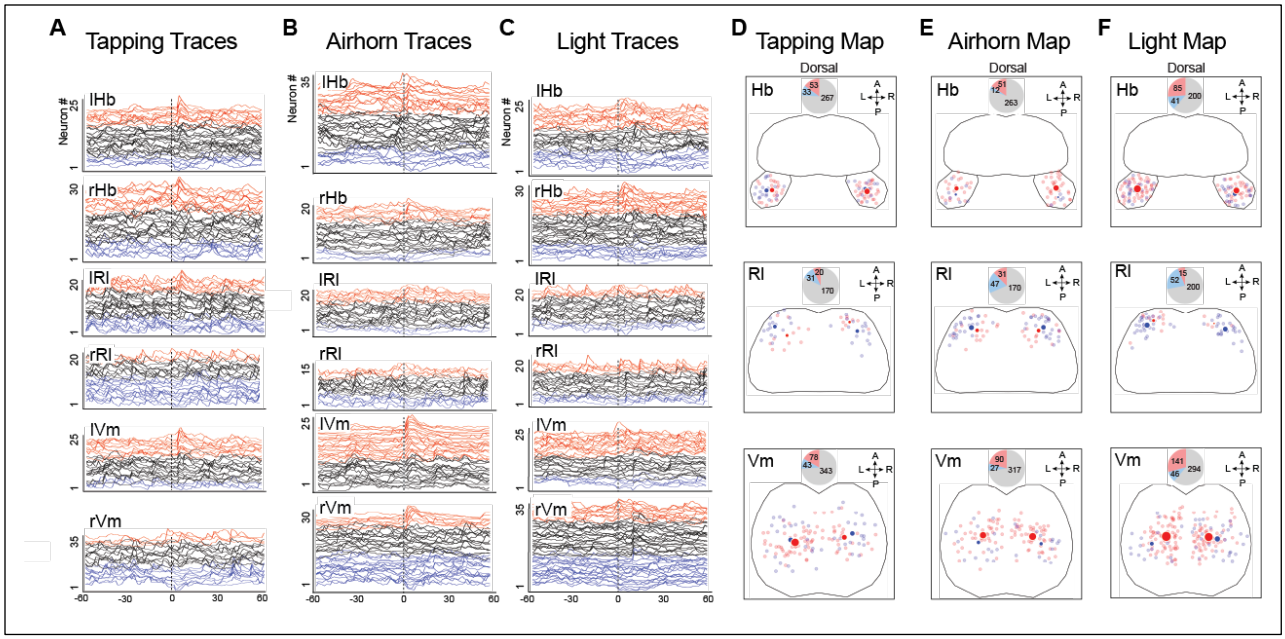

Figure 7 Response of neuronal components to vibration, a loud noise, and light

(**A**) Neuronal component ΔF/F traces of a representative fish in response to tapping at the vertical dotted line. Red denotes activation (increase in activity ≥ 50% of background ΔF/F); blue, inhibition (decrease in activity ≤ -50% of background ΔF/F); black, neither. Order is determined by z-score (μ/σ), which measures the magnitude and consistency of the response. In Hb and Vm, the responses of neuronal components to all three stimuli tend to be better defined than those in RI.

(**B, C**) Neuronal component ΔF/F traces as in (A), but in response to the blast of an airhorn (B) or a transition from light to dark (C) at the vertical dotted line.

(**D-F**) Locations of neuronal components in Hb, RI, and Vm. Small puncta mark locations where neuronal components respond by increasing (red) or decreasing (blue) activity in response to tapping (D), a blast from an airhorn (E) or a transition from light to dark (F). Large dots represent centers of mass of corresponding neuronal components. Pie graphs (inset) show the number of activated (red), inhibited (blue), and unresponsive (grey) neuronal components. Note that in RI, inhibited neurons dramatically outnumber activated neurons, whereas in Hb and Vm, the proportion of activated components are roughly equal to or greater than that of inhibited components.

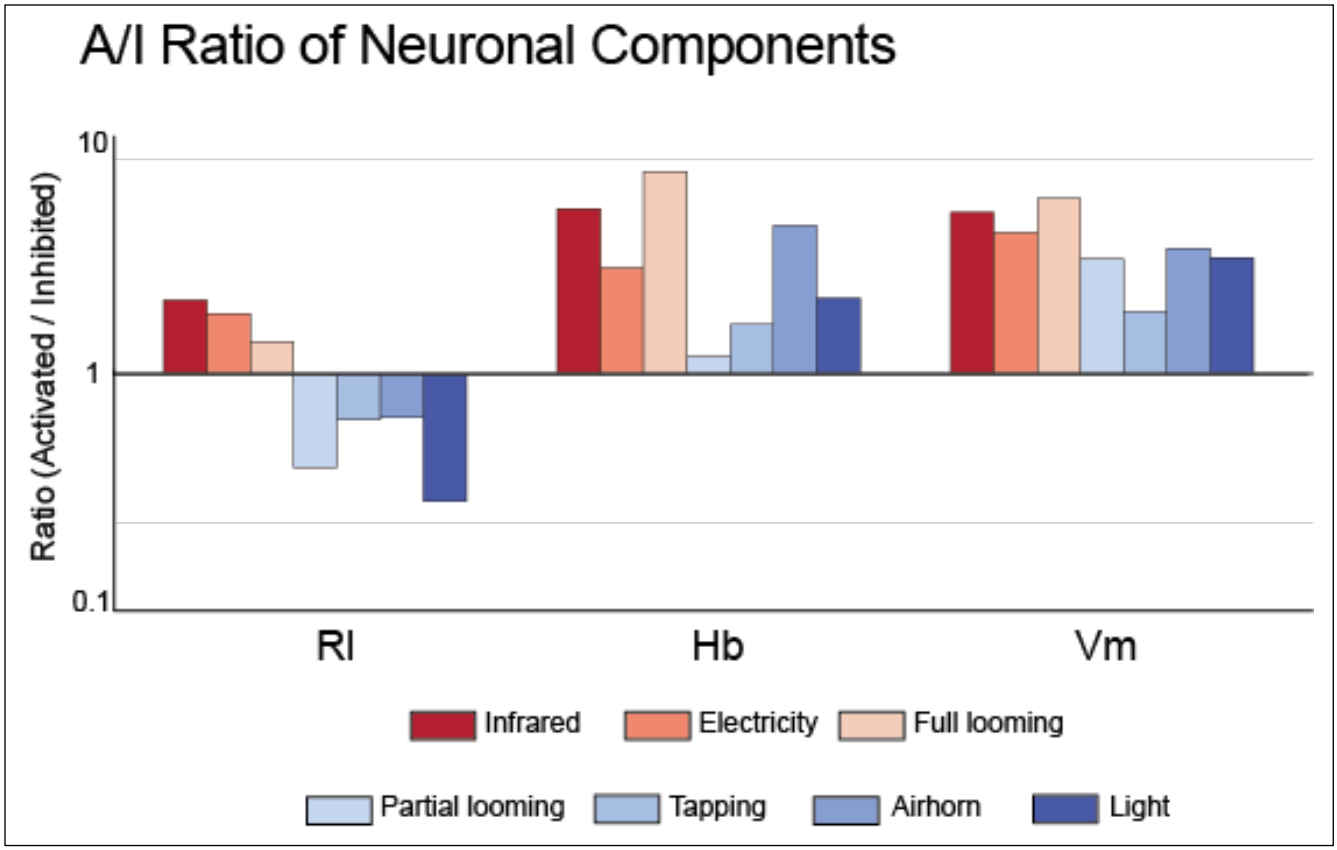

Figure 8 RI is activated by highly threatening stimuli but not by mildly threatening stimuli.

The ratio of activated to inhibited neuronal components (A/I) in RI is greater than 1 for highly threatening stimuli but less than 1 for mildly aversive stimuli. In contrast, in Hb and Vm, the A/I ration is greater than one for all aversive stimuli.

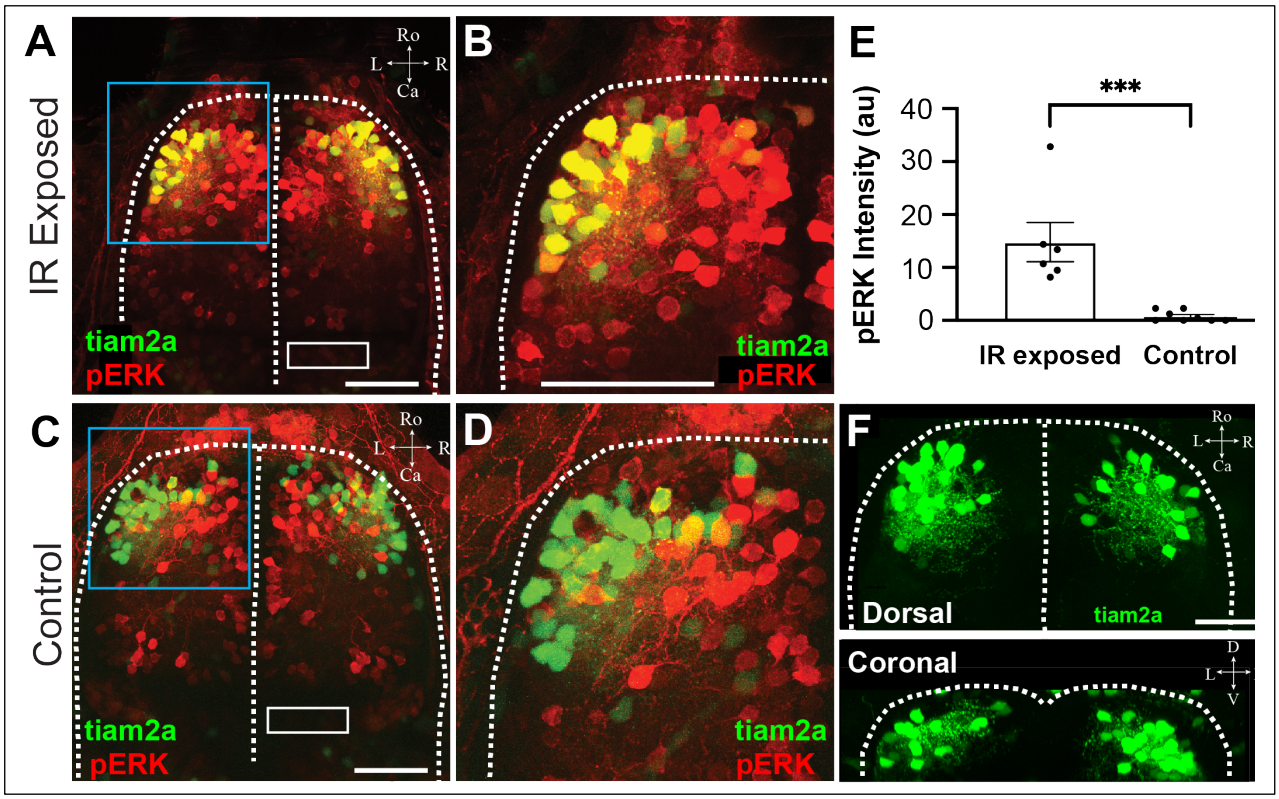

Figure 9 Cells expressing tiam2a become active when exposed to IR heating.

(**A**) 7 dpf Tg[Tiam2a::GFP] larval zebrafish exposed 10 times to heating with an IR laser and then immunostained for pERK to label active neurons. Virtually all GFP-positive neurons were co-labeled with pERK, suggesting that Tiam2a-positive cells are activated by a painful stimulus.

(**B**) Close-up of the area bordered by the blue rectangle in (A).

(**C**) 7 dpf Tg[Tiam2a::GFP] larval zebrafish control that was not exposed to heating showed very little overlap between GFP labeling and labeling for pERK.

(**D**) Closeup of the area bordered by the blue rectangle in (C).

(**E**) Average intensity of pERK immunostaining in Tiam2a+ cells, with background (measured in the white rectangle in (A)) subtracted, for fish exposed to IR heating (n = 6) and control fish (n = 8). Significantly more labeling was found in fish exposed to heating (P = 0.0009, t-test) vs. in control fish.

(**F**) Tg[Tiam2a::GFP] fish showing cell bodies concentrated in the rostrolateral area and local axonal connections.